Biochimica et Biophysica Acta 1793 (2009) 806–816

Contents lists available at ScienceDirect

Biochimica et Biophysica Acta

journal homepage: www.elsevier.com/locate/bbamcr

# ARHGAP21 modulates FAK activity and impairs glioblastoma cell migration

Carolina Louzão Bigarella, Luciene Borges, Fernando Ferreira Costa, Sara Terezinha Olalla Saad *

*Department of Internal Medicine, School of Medical Science, Hematology and Hemotherapy Center – Hemocentro, University of Campinas - UNICAMP, Campinas, São Paulo 13083-970, Brazil*

ARTICLE INFO

*Article history:*
Received 8 September 2008
Received in revised form 8 January 2009
Accepted 13 February 2009
Available online 4 March 2009

*Keywords:*
ARHGAP21
Glioblastoma multiforme (GBM)
FAK
Migration

ABSTRACT

Glioblastoma multiforme is highly aggressive and is the most common glial tumor type. Although there have been advances in treatment, the average survival expectancy is 12–15 months. Several genes have been shown to influence glioblastoma progression. In the present work, we demonstrate that the RhoGTPase Activating Protein 21 (ARHGAP21) is expressed in the nuclear and perinuclear regions of several cell lines. In T98G and U138MG, glioblastoma derived cell lines, ARHGAP21 interacts with the C-terminal region of Focal Adhesion Kinase (FAK). ARHGAP21 depletion by shRNAi in T98G cells alters cellular morphology and increases: FAK phosphorylation states and activation of downstream signaling; the activity state of Cdc42; the production of metalloproteinase 2 (MMP-2) and cell migration rates. These modifications were found to be mainly due to the loss of ARHGAP21 action on FAK and, consequently, the activation of downstream effectors. These results suggest not only that ARHGAP21 might act as a tumor suppressor gene, but also indicate that ARHGAP21 might be a master regulator of migration having a crucial role in controlling the progression of different tumor types.



## 1. Introduction

The Rho-family GTPases are the main regulators of actin cytoskeleton dynamics [1]. These molecules cycle between an active GTP-bound form and an inactive GDP-bound form. This cycle is controlled by guanine nucleotide exchange factors (RhoGEFs), positive regulators that promote the release of bound GDP and facilitate GTP binding [2], guanine nucleotide dissociation inhibitors (RhoGDIs), which sequester the GDP-bound form of RhoGTPase and may also regulate their intracellular localization [3], and by GTPase activating proteins (RhoGAPs), negative regulators that increase the intrinsic GTPase activity of the RhoGTPase [4].

Currently, over 70 RhoGAP proteins encoded by the human genome have been described [5]. An important member is ARHGAP21, a protein identified in a Brazilian cancer EST database that contains, in addition to its RhoGAP domain, a Pleckstrin Homology domain (PH) and a *P*SD-95/*D*iscs-large/*Z*O-1 (PDZ) domain [6]. As PDZ domains are commonly conserved protein–protein interaction domains found in organisms ranging from bacteria to humans [7] and as the modular structures of GAPs are important for their interaction with other proteins [5], ARHGAP21 is thought to have additional functions other than the negative control of RhoGTPases. In fact, recently, ARHGAP21 was shown not only to have preferential GAP activity over Cdc42, but also to bind to ARF1-GTPase to control vesicular trafficking on Golgi membranes, and to interact with α-catenin, recruiting this protein to endothelial sites of bacterial invasion [8]. Thus, ARHGAP21 is being characterized as a controller of actin cytoskeleton dynamics.

Glioblastoma multiforme (GBM; astrocytoma WHO grade 4) is a highly malignant brain tumor that accounts for over 50% of all glial tumor types, with a median survival rate of under 1 year [9]. Current treatments of these tumors include surgery followed by radiation and chemotherapy with highly toxic, non-specific agents [10]. The key contributor to treatment failure is the high capacity of malignant gliomas to infiltrate and invade adjacent brain structures, which renders surgical removal difficult [11]. Therefore, if novel targets for therapy design are to be identified, a better understanding of the molecular mechanisms that control glioblastoma cell migration is imperative.

Given the importance of RhoGAPs in inhibiting actin dynamics and the high levels of ARHGAP21 in the normal human brain [6], we postulated that ARHGAP21 might play an important role in glioblastoma cell migration. In agreement with our hypothesis, we found that ARHGAP21 interacts with the Focal Adhesion Kinase (FAK) in glioblastoma cell lines (T98G and U138MG), and that its knockdown in T98G cells leads to increased cellular migratory properties; furthermore, the pathways leading this event are mediated by FAK and Cdc42 increased activity states. Our results identify ARHGAP21 as

* Corresponding author. Department of Internal Medicine, Hematology and Hemotherapy Center, University of Campinas, Rua Carlos Chagas 480, Cidade Universitária Zeferino Vaz, Barão Geraldo, CEP 13083-970, Caixa Postal 6198, Campinas-SP, Brazil. Fax: +55 19 3289 1089.
*E-mail addresses:* carolbiga@yahoo.com.br (C.L. Bigarella), sara@unicamp.br (S.T.O. Saad).

0167-4889/$ – see front matter © 2009 Elsevier B.V. All rights reserved.
doi:10.1016/j.bbamcr.2009.02.010

a novel inhibitor of glioblastoma cell migration and suggest that ARHGAP21 might function as a metastasis suppressor in glioblastoma multiforme.

## 2. Materials and methods

### 2.1. Nomenclature

Gene symbols used in this article follow the recommendations of the HUGO Gene Nomenclature Committee [12].

### 2.2. Reagents and antibodies

Polyclonal antibody against ARHGAP21 was generated against a synthetic peptide (KSDSGSLGDAKNEKE), corresponding to residues 1856–1870 of the human protein and affinity purified by Bethyl Laboratories, Inc. (Montgomery, Texas). Rabbit polyclonal antibodies against FAK, c-Src, $p130^{CAS}$ and Histone-H1, monoclonal anti-Cdc42, and goat polyclonal antibody against P-FAK Tyr925 was purchased from Santa Cruz Biotechnology (Santa Cruz, CA). Rabbit polyclonal antibodies against P-Src Tyr418 and P-FAK Tyr397 were purchased from Biosource (Bethesda, MD). Phalloidin-TRITC was purchased from Sigma (St Louis, MO). Anti-transferrin receptor (Tr) is from Zymed Laboratories Inc. (San Francisco, CA). AlexaFluor® 488, AlexaFluor® 633 and AlexaFluor® 555 conjugated secondary antibodies and ProLong® Gold antifade reagent with DAPI were from Molecular Probes (Eugene, OR). Enhanced chemiluminescence reagents were obtained from GE Health Care (Buckinghamshire, UK). All other reagent grade chemicals were obtained from Sigma.

### 2.3. Cell culture

The human glioblastoma derived cell lines, A172, T98G and U138MG, and the cervical carcinoma cell line HeLa were obtained from the American Type Culture Collection (ATCC). The short-term culture of normal human fibroblasts was established from the skin of a mammary reduction surgery, in accordance with the Helsinki Declaration Guideline of 1975 (reviewed in 1983) at Dr. Gláucia Santelli Laboratory (ICB, University of São Paulo, São Paulo, Brazil). All cell lines were maintained in Dulbecco's modified Eagle's medium (DMEM) with 4 mM L-glutamine, adjusted to contain 1.5 g/L sodium bicarbonate and 4.5 g/L glucose, supplemented with 10% fetal bovine serum (Gibco-Invitrogen) in an atmosphere of 5% $CO_2$–air at 37 °C.

### 2.4. Cell fractionation

A172, T98G and HeLa cells were cultivated until reaching the desired confluence and then collected in buffer A (10 mM Hepes pH 7.9, 1.5 mM $MgCl_2$, 10 mM KCl, 0.5 mM DTT, sodium orthovanadate, aprotinin and PMSF). Cell pellet was ressuspended in buffer A plus 0.1% NP-40 and homogenized with an insulin syringe 20 times for membrane disruption. Nuclear-, membrane- and cytoplasm fractions (pellet and supernatant, respectively) were separated by centrifugation. The supernatants were centrifuged for 1 h at 100,000 ×*g* to fractionate membrane (pellet) and cytoplasm fractions. The membrane fraction was ressuspended in buffer A plus 0.1% Triton-X-100 and the nuclei fraction was ressuspended in buffer B (20 mM Hepes, pH 7.9; 1.5 mM $MgCl_2$; 0.5 mM DTT, 25% glycerol; 0.2 mM EDTA; 0.42 M NaCl; sodium orthovanadate; aprotinin). 100 μg of protein extract of the cytoplasm fraction and the corresponding percentage of the other extracts were fractionated in SDS-PAGE.

### 2.5. Generation of ARHGAP21-knockdown cells

Small hairpin type RNAi oligonucleotides (shRNAi) were designed using the Ambion inc. web site. The sequences were cloned into the expression vector, p*Silencer* 2.1 U6 neo™ (Ambion Inc, Austin, TX), following the manufacturer's instructions. The shRNAi sequences used to silence the *ARHGAP21* human gene (GenBank accession number NM-020824) in T98G glioma cell line were *sh1*: GATCCCGCACGTACCTAGTCTGAAGTTCAAGAGACTTCAGACTAGGTACGTGCTTTTTTGGAAA and *sh2*: GATCCCGTATTCGGCCATGGAAACATTCAAGAGATGTTTCCATGGCCGAATACTTTTTTGGAAA. As a control for shRNAi, we used a plasmid of the Ambion kit that contained a shRNAi with no homology to human, mouse or rat genomes. Briefly, T98G cells were transfected with p*Silencer*™ plasmid containing the control or *ARHGAP21*-shRNAi using Lipofectamine 2000® (Invitrogen Inc, Carlsbad, CA) transfection reagent, following the manufacturer's instructions. Four hours later, medium containing 20% FBS was added (to a final concentration of 10%); after 24 h, the transfection medium was changed to 10% FBS DMEM, and 48 h later, the cells were harvested and divided in 100 mm dishes to start clone selection using 500 μg/mL of G418 (Gibco-Invitrogen Inc, Carslbad, CA).

### 2.6. Phase contrast imaging

Fixed cell images were acquired with a Nikon Eclipse E600 microscope equipped with light, epifluorescence illumination and a high-resolution CCD camera (RT Slider, Diagnostic Instruments, Inc., Sterling Heights, MI, USA) and a PC running Image-Pro software (Media Cybernetics, Inc., Silver Spring, MD, USA), using the 200× objective. Pictures shown are representative of the morphology changes of all analyzed clones.

### 2.7. Confocal immunofluorescence microscopy

Confocal imaging was carried out using primary antibodies against ARHGAP21, Cdc42, FAK and P-FAK Y925 (diluted 1:100) or TRITC-Phalloidin. Briefly, $2 \times 10^4$ cells were plated on coverslips. Cells were fixed in 4% paraformaldehyde-PBS for 20 min and then permeabilized with 0.5% Triton-X-100 in PBS for 10 min. The cells were blocked with 3% skimmed milk-PBS and then incubated with the indicated primary (overnight, 4 °C) and secondary (1 h, room temperature) antibodies, and with phalloidin-TRITC (dilution 1:500) for 30 min. Finally, coverslips were mounted on slides using the ProLong Gold® antifade reagent and the cells were analyzed by confocal laser scanning in a LSM 510 (Zeiss, Welwyn Garden City, UK) mounted over an Axioplan microscope (Zeiss) using 40× or 63× 1.3 NA oil immersion objectives. In order to compare signals from different stained proteins, the pinhole aperture was fixed. FAK and Cdc42 staining reproduced results, which were found in all analyzed *ARHGAP21*-inhibited clones. For the quantification of ARHGAP21/FAK colocalization (shown in Fig. 2B), we used the "colocalization finder" plug in of ImageJ free image analysis software (W. Rasband, National Institutes of Health, Bethesda; http://rsb.info.nih.gov/ij/). And for the quantification of Cdc42 displacement due to ARHGAP21 depletion we counted how many T98G NC ($n = 601$), sh1 ($n = 477$) and sh2 ($n = 730$) cells showed the Cdc42 localization changes. Data was analysed using Kruskal–Wallis test of the GraphPad-Prism software.

### 2.8. Immunoprecipitation and immunoblotting

T98G and *ARHGAP21*-knockdown cell lysates were prepared in RIPA buffer containing protease inhibitors, as previously described [13]. Briefly, 500 μg of total T98G cell extracts was incubated overnight with 5 μg of the specified antibodies or with normal rabbit immunoglobulin (IgG) as a negative control. The immune complexes were precipitated with protein-A-sepharose 50% slurry (GE), washed in RIPA buffer to remove unspecific proteins that might be bound to the complex, and then analyzed by 8% SDS-PAGE and immunoblotting with the antibodies of interest. Data from immunoprecipitation experiments is representative of at least three independent experiments.

### 2.9. Pulldown assay

pGEX2T, carrying the portion of the FAK amino-terminal domain (GST-FERM; residues 1 to 400), pGEX2TK, encoding the fusion protein C-terminal of FAK (GST-C-term; residues 765 to 1,052), and pGEX-KG, containing the cDNA sequence of the catalytic domain (GST-CAT; residues 400 to 396), were a kind gift from Jun-Lin Guan from the Department of Molecular Medicine of Cornell University, Ithaca, NY (FERM domain), and Michael Schaller from the Department of Microbiology and Cancer Center of the University of Virginia School of Medicine (CAT and C-terminal domains). All constructions were inserted into *Escherichia coli* BL21 (RIL) Codon Plus and performed as previously described [14,15], except for minor modifications. Glutathione beads, conjugated with the three different GST recombinant proteins, were used for the pulldown assay on T98G cells lysed in GST-Fish buffer plus protease inhibitors [16]. The pulled down pellets were resolved in SDS-PAGE gel and the membranes were probed with anti-ARHGAP21 or anti-Src antibodies.

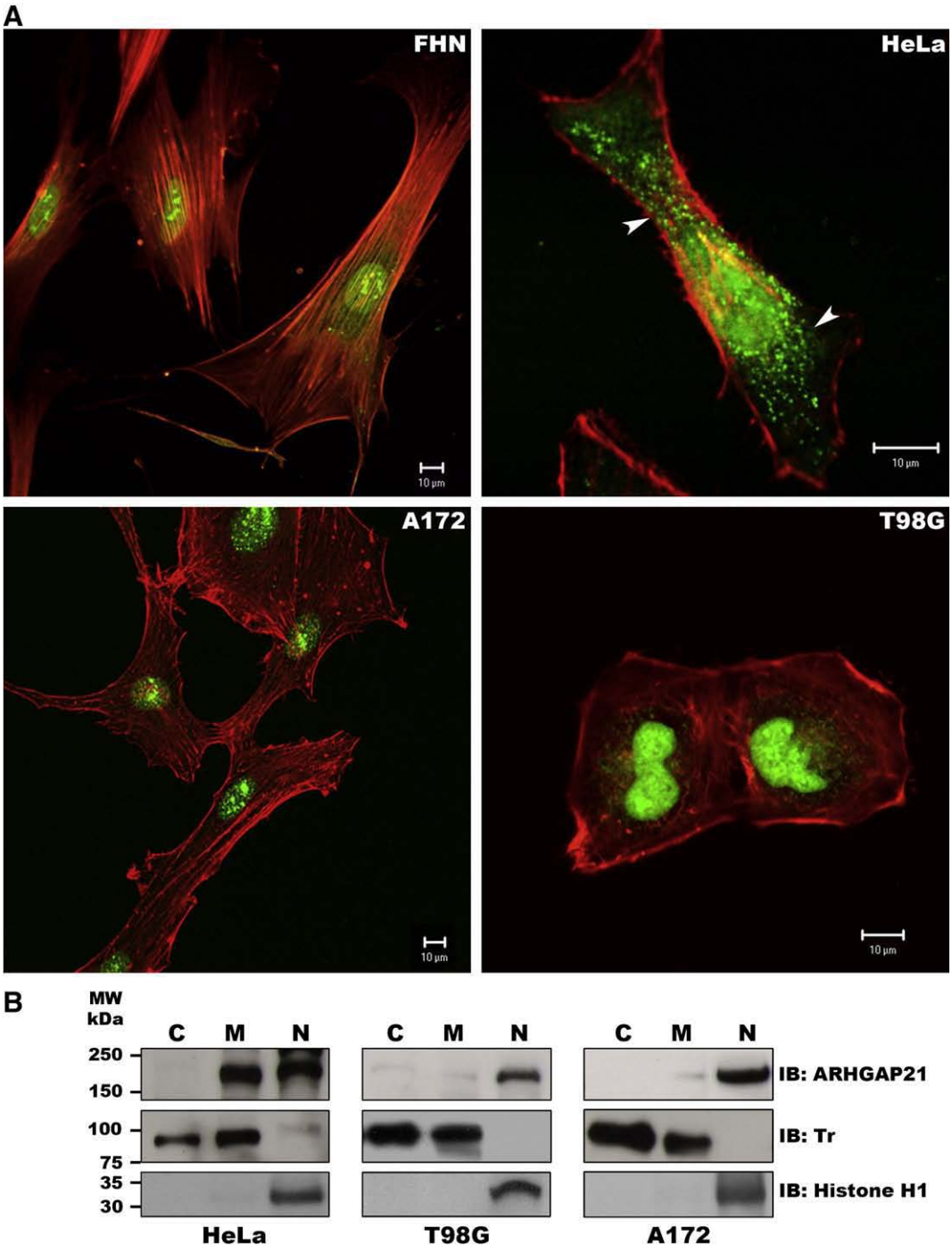


**Fig. 1.** Nuclear localization of ARHGAP21. (A) Confocal micrographs of FHN, HeLa, A172 and T98G cell lines displaying ARHGAP21 (green) and F-actin (red) staining using 40× (FHN and A172) and 63× (HeLa and T98G) oil immersion objectives. (B) Cell fractionation of HeLa, T98G and A172 cell lines, which confirms the nuclear and perinuclear (arrow heads) localization of ARHGAP21. The efficiency of the fractionation was verified by transferring receptor (Tr) and Histone H1 blots, which should be, respectively, cytoplasm and membrane, and nuclear localized. C = cytoplasm; M = membrane and N = nuclei. (For interpretation of the references to colour in this figure legend, the reader is referred to the web version of this article.)

*2.10. Cdc42 activity assay*

The activity of Cdc42 was determined by affinity–precipitation assay. The Cdc42 WASP-binding domain (amino acids 215 to 295) cloned in pGEX-KG was a kind gift from Dr. David Sacks from Brigham and Women's Hospital, Boston, and was expressed as previously described [17]. T98G NC and T98G-*ARHGAP21*-knockdown cells were lysed in GST-Fish buffer (10% glycerol, 50 mM Tris pH 7.4, 100 mM NaCl, 1% NP-40, 2 mM $MgCl_2$, 10 μg/mL aprotinin, 1 mM phenylmethylsulfonyl fluoride, 1 mM sodium orthovanadate and 1 μg/mL leupeptin). Five-hundred μg of total proteins were incubated with 100 μg GST-WBD beads, for 90 min at 4 °C. Cdc42-WBD complexes were fractionated in SDS-PAGE and membranes were probed with anti-Cdc42 monoclonal antibody. Cdc42-GTP (Cdc42-WBD) was

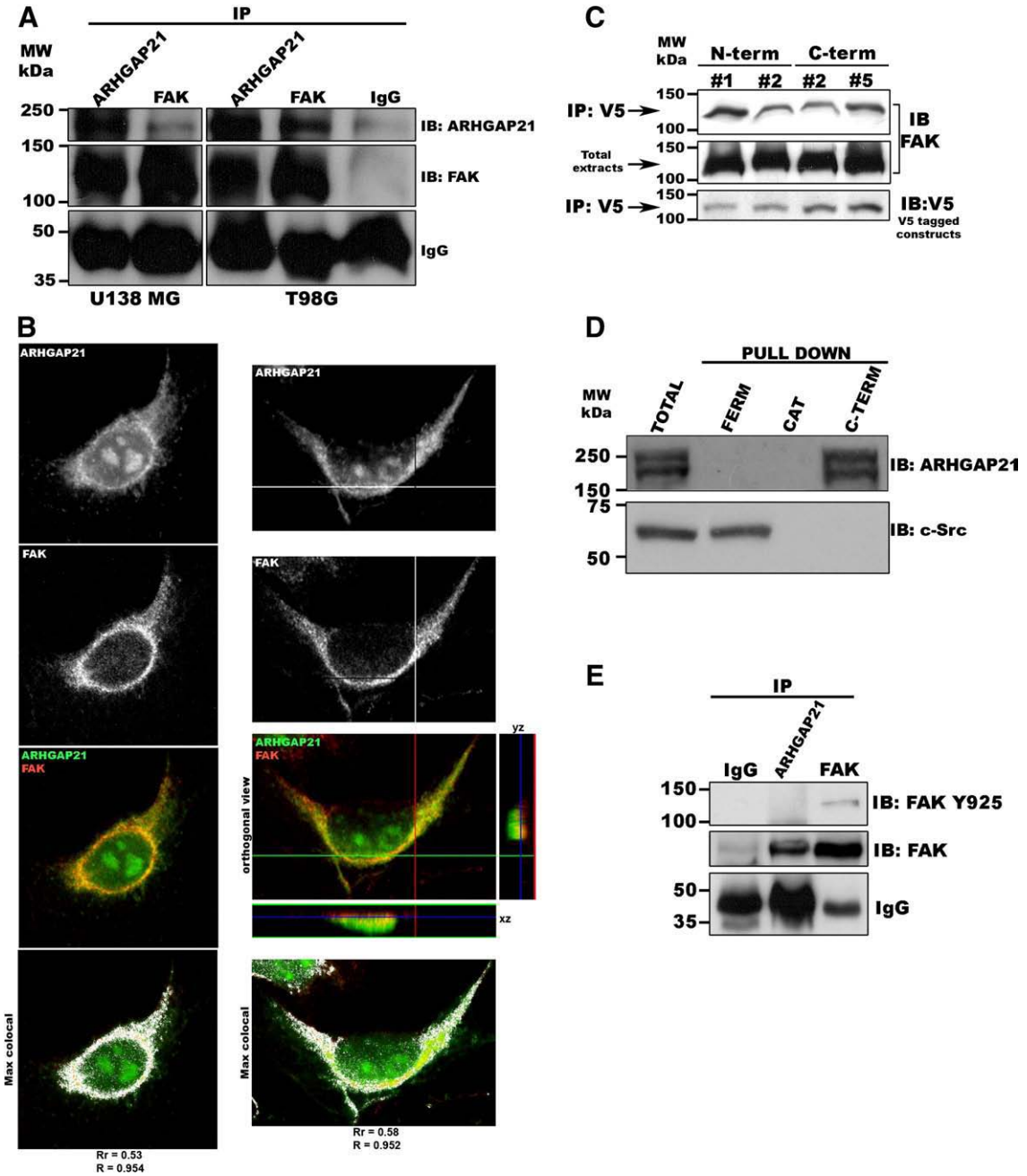


**Fig. 2.** ARHGAP21 interacts with FAK on U138MG and T98G glioblastoma cell lines. (A) Cell lysates from U138MG and T98G were co-immunoprecipitated with normal rabbit-IgG, anti-ARHGAP21 or anti-FAK antibodies and the associated proteins were analyzed by immunoblotting with the same antibodies. (B) Immunofluorescence staining of ARHGAP21 (green) and FAK (red) showing colocalization of those proteins in the perinuclear area. Colocalization analysis was performed with the Colocalization Finder plug in of ImageJ NIH software and shows merged images of FAK (red) and ARHGAP21 (green), with colocalized pixels in white. Pearson's correlation coefficient (Rr) and Overlap coefficient (*R*) are shown below each merged image. The merged panel of the second column has orthogonal projections of the overlapping proteins. (C) Two clones of T98G cells stable transfected with V5-tagged N-terminus or C-terminus portions of ARHGAP21 were immunoprecipitated with anti-V5 and immunoblotted with anti-FAK. Results demonstrate the interaction of FAK with both regions of ARHGAP21. (D) Pulldown assay of T98G cell extracts using constructions of FERM, Catalytic (CAT) and C-terminal (C-TERM) domains of FAK. (E) T98G cell extracts were immunoprecipitated with normal rabbit-IgG, anti-ARHGAP21 or anti-FAK antibodies and the interaction with active FAK was analyzed by immunoblotting with anti-FAKY925. Immunoblotting with anti-FAK was used to show that FAK precipitation was successful. IP = immunoprecipitation, IgG = normal rabbit immunoglobulin, IB = immunoblotting. Confocal images were taken using the 40× water immersion objective. Max colocal. = areas of maximal colocalization between FAK and ARHGAP21. FAK GST-constructs: FERM = N-terminus domain; CAT = catalytic domain and C-TERM = C-terminus domain. (For interpretation of the references to colour in this figure legend, the reader is referred to the web version of this article.)

compared to total Cdc42 content of cell extracts. Activity assay was performed with clones obtained from three independent transfections and all showed increased Cdc42-GTP.

### 2.11. Migration assay

T98G NC and *ARHGAP21*-knockdown cells were submitted to migration assays in Costar transwells (8 μM pore membrane). Briefly, polycarbonate membranes were incubated with 1 mg/mL of poly-L-lysine in DMEM for 2 h at 37 °C and then washed with dd-water. Synchronized cells (grown for 24 h in the absence of serum) were harvested, counted and $5\times10^4$ cells were plated per membrane. Medium containing 10% FBS and medium without serum in the lower compartment of the transwells were used as chemo-attractant and control, respectively. After 48 h, cells were fixed in 5% glutaraldehyde-PBS and stained with 1% toluidine blue [18]. Cells on the upper side of the membrane were removed with a cotton-swab. The membranes were dried, the dye was eluted with 1% SDS and the amount of cells on the lower side of the membrane (migrated cells) was estimated by its absorbance at 595 nm, as a function of total cell absorbance (membranes without upper side cells removed). At least two independent experiments were performed using triplicates for all conditions. Wilcoxon Rank Sum Test was used to analyze data from migration experiments (two independent samples) using the BioEstat software. Results are shown as mean ± SD.

### 2.12. Gelatin zymography

T98G and *ARHGAP21*-knockdown cells were plated ($1\times10^5$ cells/well) in 12-well plastic plates or in wells prior containing a thin layer of 5 mg/mL Matrigel™ (BD Biosciences, Bedford, MA). Cells were grown for 48 h and then the culture medium was replaced by DMEM without serum. Forty-eight hours later, the medium was collected and clarified by centrifugation and the cells of each well were counted. A volume of supernatant corresponding to $1\times10^4$ cells was applied to each lane of a 7.5% SDS-PAGE containing 0.1% gelatin. The gel was then washed in a Triton-X-100 buffer to remove traces of SDS and then in water to remove Triton. The gel was incubated in zymography buffer for 24 h (37 °C). Finally, the gel was left staining in Coomassie-brilliant blue for 16–18 h and destained for 2 h. Zymography experiments have been performed with clones obtained in all three independent transfections and similar results were found.

## 3. Results

### 3.1. Subcellular localization of ARHGAP21

ARHGAP21 localizes to the nuclei and perinuclear region of normal human fibroblasts (FHN), glioblastoma cell lines A172 and T98G and the cervical carcinoma cell line, HeLa (Fig. 1A), which corroborates previous work from our lab [19]. In addition, the presence of ARHGAP21 in the nuclear fraction of all cell lines was also observed in cellular lysates of A172, T98G and HeLa cells, which we submitted to fractionation (Fig. 1B). The presence of ARHGAP21 in the membrane fraction of HeLa cells is probably due to its presence in perinuclear vesicular compartment that precipitates together with the membrane fraction (Fig. 1A, arrow heads). The efficacy of the fractionation protocol was checked by subcellular distribution of the transferrin receptor, a known cytoplasmic and membrane protein (Tr), and of Histone H1, a known nuclear protein.

The specificity of ARHGAP21 polyclonal antibody was evaluated by immunoprecipitation, shRNAi and blotting with the antibody and rabbit pre-immune serum (Supplementary material, Sup. Figs. 1A and B), and immunofluorescence negative controls were carried out using rabbit pre-immune serum and the respective secondary antibody (Supplementary material, Sup. Fig. 2B).

### 3.2. ARHGAP21 interacts with the C-terminal portion of FAK

In order to investigate the involvement of ARHGAP21 in the integrin-signaling pathway that mediates extracellular matrix

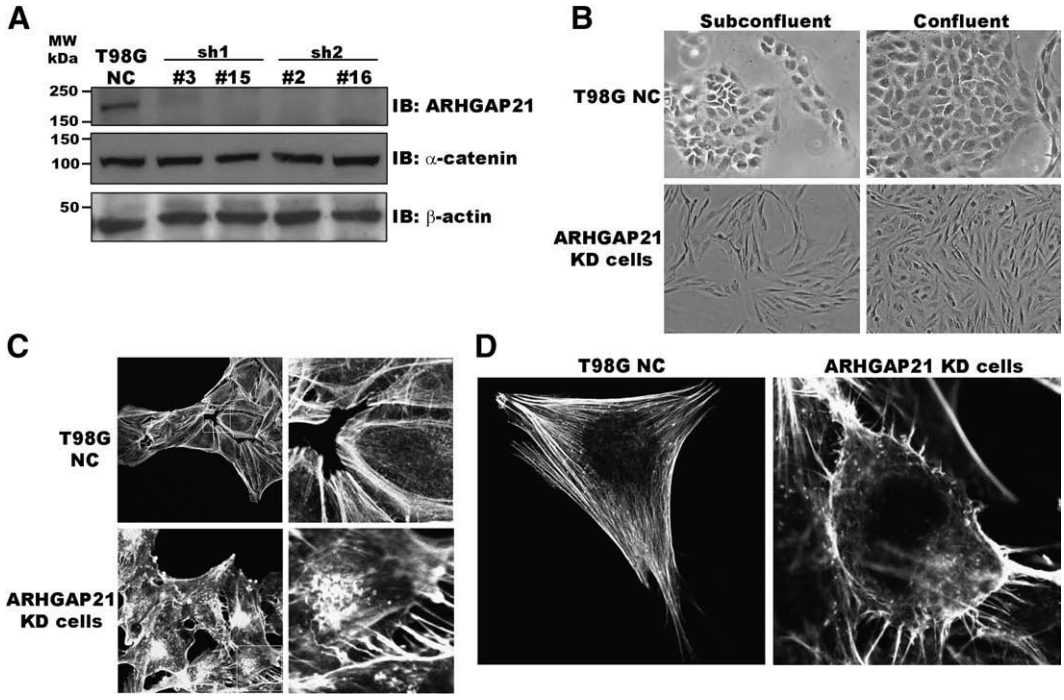


**Fig. 3.** ARHGAP21 depletion results in morphological and cytoskeleton changes. (A) immunoblotting of cell lysates from T98G NC (negative control) and T98G-*ARHGAP21*-knockdown cells (KD), resulting from the stable transfection of two different shRNAi. Antibodies against β-actin and α-catenin were used as controls of to show the equal protein loading. (B) Representative optical micrographs (200× magnification) and (C) confocal imaging (40× oil immersion objective) of actin cytoskeleton stained with phalloidin-TRITC, showing the morphological and cytoskeleton re-organization in T98G-*ARHGAP21*-knockdown cells (KD cells). (D) Pictures of zoomed individual cells are shown in higher magnification (63×) evidencing F-actin alterations.

adhesion, we performed co-immunoprecipitation assays in T98G and U138MG cell lines of the endogenous ARHGAP21 with several known cytoskeletal proteins and found the protein to interact with the Focal Adhesion Kinase (FAK) (Fig. 2A), a master regulator of integrin signaling known to regulate RhoGAPs [1]. Confocal micrographs displayed that the interaction between these proteins occur in the perinuclear region (colocalization zones displayed in yellow and white dots generated by the "Colocalization Finder" plug in from ImageJ software, Fig. 2B) and quantitatively displays a high overlapping coefficient. T98G stable transfected clones expressing constructs of ARHGAP21-V5 tagged N-terminus (#1 and #2) or C-terminus (#2 and #5) showed that the interaction between ARHGAP21 and FAK can be mediated by both portions of ARHGAP21 (Fig. 2C), as the overlapping region of those constructs comprises only 47 amino acids and neither of the domains [20]. Further confirmation of an ARHGAP21-FAK complex came from pulldown assays using different FAK constructs (FAK's N-terminus domain (FERM), catalytic domain (Cat) and the C-terminus-focal adhesion target domain (C-term)), which mapped ARHGAP21 specific binding to the C-terminus of FAK (Fig. 2D). Src pulldown was used as a positive control, since it is known to interact with the Tyr 397 of FAK, which is present in the FERM construct. Similar results were also found in the A172 glioblastoma cell line, MCF-7 breast carcinoma cell line and rat cardiomyocytes [19]. However, immunoprecipitation experiments in T98G cells using anti-FAK or anti-ARHGAP21 antibodies and blotting with anti-FAK-Y925 displayed that ARHGAP21 does not interact with FAK when Tyr925 is phosphorylated (Fig. 2E).

### 3.3. T98G-ARHGAP21-knockdown cells display altered morphology and actin cytoskeleton appearance

T98G glioblastoma cells were transfected three times, independently, and results herein are representative of all transfections. Plasmids (p*Silencer* 2.1 U6 neo® — Ambion) containing short-hairpins interfering RNA (shRNAi) directed to silence the *ARHGAP21* human gene or control-ones were used. Several stable inhibited clones (named "#") were selected. Depletion of ARHGAP21 was demonstrated in four selected clones that achieved almost total depletion of ARHGAP21, demonstrated by protein levels (Fig. 3A). As a control of protein levels, we used β-actin and α-catenin, a known binding protein of ARHGAP21 [20]. The inhibition triggered morphological changes, which are similar to an epithelial to mesenchymal transition (Fig. 3B), and actin cytoskeleton changes from bundled, cortical actin to a disarranged pattern displaying accumulation of actin in the perinuclear region and the formation of membrane protrusions (Figs. 3C, zoomed areas and d, higher magnification of individual cells).

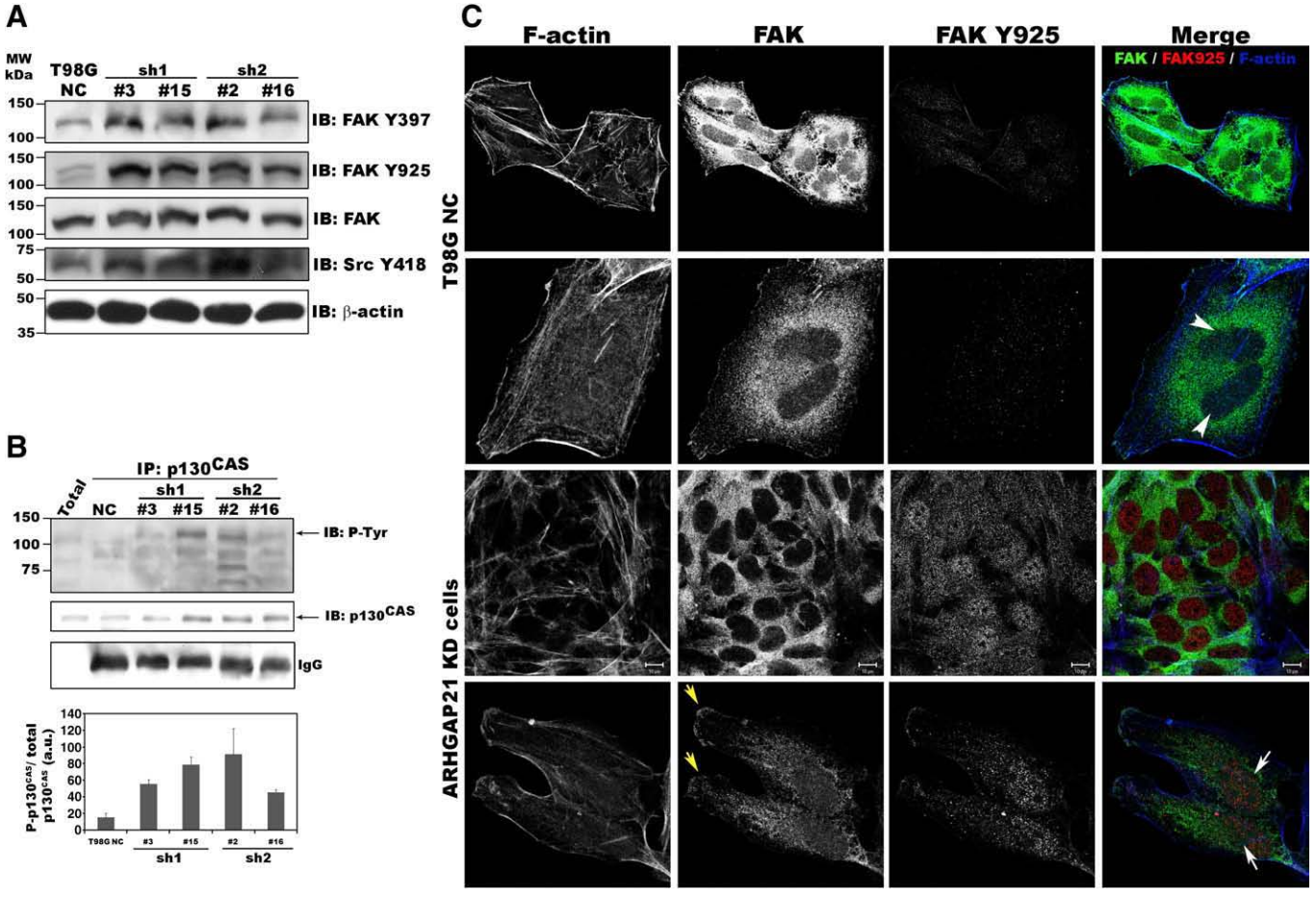


**Fig. 4.** ARHGAP21 knockdown increases phosphorylation states of FAK and the downstream effector, p130$^{CAS}$. (A) Immunoblotting of T98G NC and four selected inhibited *ARHGAP21*-knockdown clones with anti-P-FAK Y397, anti-P-FAK Y925 and anti-P-Src Y418 antibodies, demonstrating the increased phosphorylation of tyrosine sites. (B) Immunoprecipitation of p130$^{CAS}$ and immunoblotting with anti-P-Tyr; quantitation of the P-p130$^{CAS}$ content was normalized in relation to the total p130$^{CAS}$ precipitated and showed the increased phosphorylation of p130$^{CAS}$ on *ARHGAP21*-knockdown clones (graphic). (C) Confocal imaging of T98C-NC and of a representative *ARHGAP21*-knockdown clone (KD cells) in group or isolated, demonstrating the augment in FAK Y925 staining and nuclear localization due to ARHGAP21 knockdown (white arrow heads on T98NC showing empty nuclei and white arrows displaying FAKY925 nuclear accumulation on KD cells). Yellow arrows show regions of membranar FAK on ARHGAP21 KD cells. IP = immunoprecipitation, IgG = normal rabbit immunoglobulin, IB = immunoblotting, NC = T98G negative control. (For interpretation of the references to colour in this figure legend, the reader is referred to the web version of this article.)

### 3.4. T98G-ARHGAP21-knockdown cells display higher FAK and Src activity levels and activation of p130$^{CAS}$ downstream signaling

We checked the activity state of FAK and its downstream effectors. Western blotting, using antibodies that recognize c-Src phosphorylated in Tyr 418 and FAK phosphorylated in Tyr 397 or Tyr 925, demonstrated that, in T98G-*ARHGAP21*-knockdown clones, c-Src displayed increased phosphorylation, as did FAK phosphorylation in autocatalytic Tyr397 and in Tyr925, when compared to T98G NC cells (Fig. 4A). These alterations may occur due to the increased FAK phosphorylation in Tyr 397, which may increase Src phosphorylation, which then phosphorylates other sites on FAK, including the Tyr925.

We also examined whether the p130$^{CAS}$ phosphorylation pattern is altered by ARHGAP21 depletion. The levels of phosphorylated p130$^{CAS}$

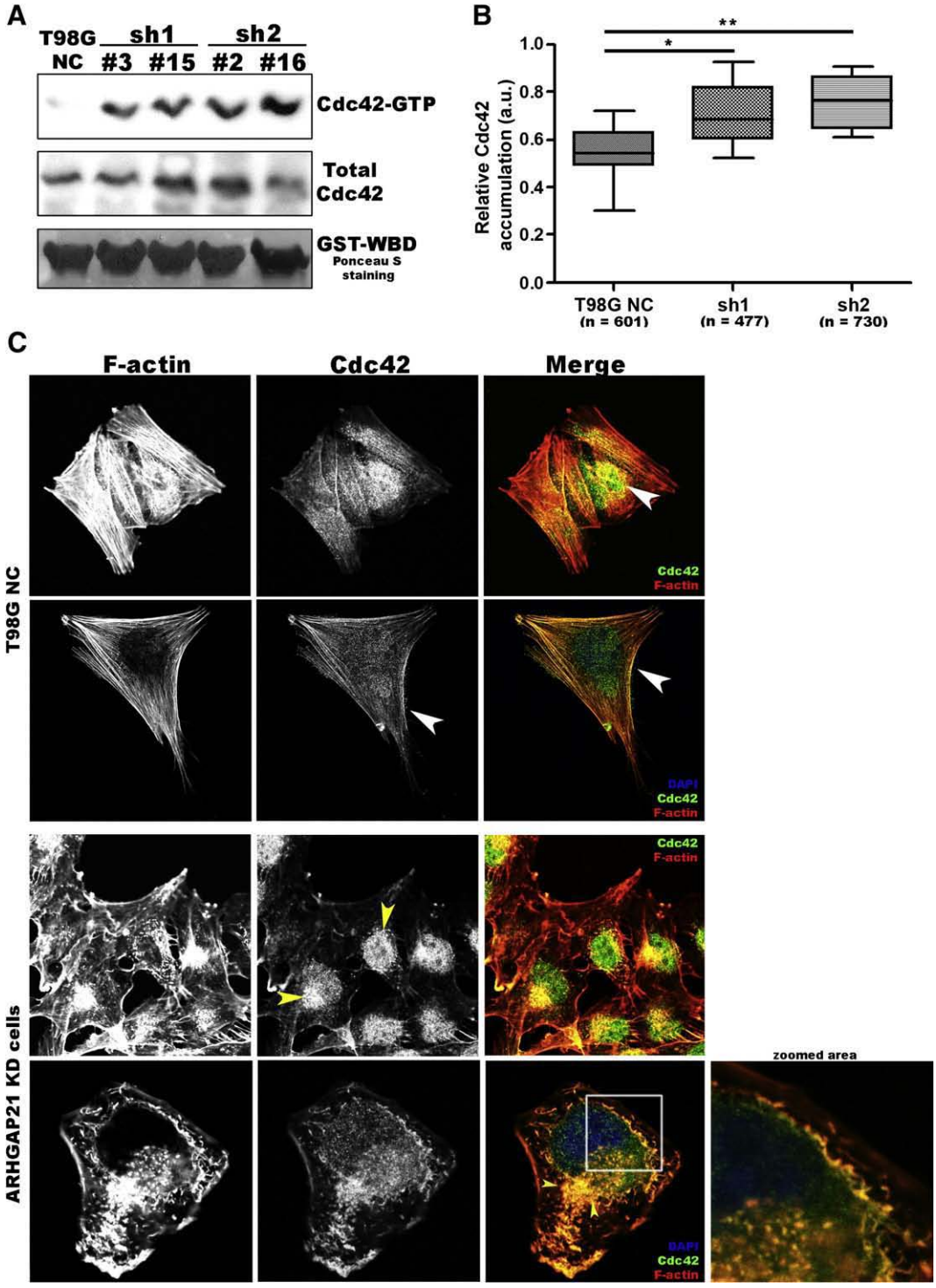


**Fig. 5.** Depletion of ARHGAP21 results in increased Cdc42-GTP and its altered localization. (A) T98G NC and T98G-*ARHGAP21*-knockdown clones were submitted to a pulldown assay of Cdc42-GTP, using the WASP-binding domain GST-fusion (GST-WBD), which evidenced higher Cdc42 activity when ARHGAP21 was depleted. (B) Quantitation of Cdc42 perinuclear accumulation evidencing the increased Cdc42 accumulation in cells where ARHGAP21 have been depleted (sh1 and sh2). (C) Confocal imaging of T98C-NC and of a representative *ARHGAP21*-knockdown clone groped or isolated showing the Cdc42 displacement due to ARHGAP21 depletion. Statistical analysis were done using the Kruskal–Wallis test of the GraphPad-Prism software. *$p<0.01$ and **$p<0.001$.

were analyzed in T98G NC and *ARHGAP21*-knockdown cells by co-immunoprecipitation assays using an antibody against $p130^{CAS}$, followed by immunoblotting with anti-P-Tyr. The amount of phosphorylated $p130^{CAS}$ has been quantified (Fig. 4B, graph) in relation to total $p130^{CAS}$ precipitated in the assay ($p130^{CAS}$ blot), and the loading has been controlled by IgG amounts. $p130^{CAS}$ displayed a 2 to 4 fold increase in tyrosine phosphorylation levels when ARHGAP21 was depleted (Fig. 4B, graph), indicating that migration pathways downstream of FAK are more active due to ARHGAP21 depletion.

Moreover, FAKY925 expression was increased in *ARHGAP21*-knockdown cells as demonstrated by immunofluorescence staining and confocal microscopy of grouped or individual cells (Fig. 4C, white arrow heads displaying empty nuclei in T98G NC cells). Interestingly, FAK phosphorylated in Tyr925 was also present in the nuclear compartment (Fig. 4C, white arrows).

### 3.5. ARHGAP21 depletion increases Cdc42 activity and alters Cdc42 subcellular distribution

ARHGAP21 is known to have GAP activity against Cdc42 [8] and RhoA [20]. Thus, we determined the activity state of Cdc42 and RhoA when ARHGAP21 was depleted. For this purpose, a pulldown assay was used with constructs comprising the Wiskott–Aldrich syndrome protein-binding domain for active Cdc42 (GST-WBD) and the rhotekin-binding domain for active RhoA (GST-WBD). No RhoA activity was detected in either parental T98G cell or ARHGAP21

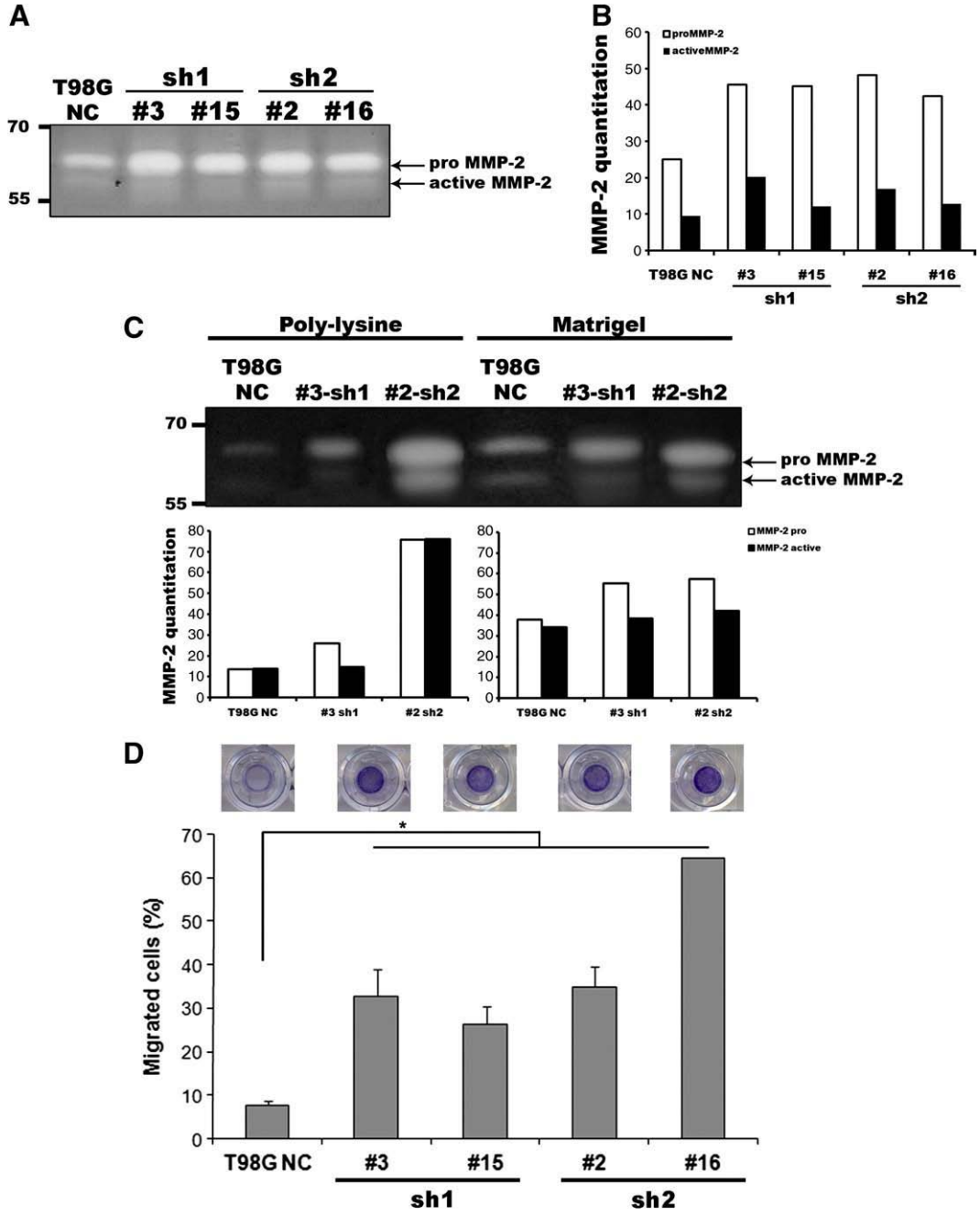


**Fig. 6.** Depletion of ARHGAP21 results in increased MMP-2 secretion and higher migration rates. (A) Gelatin zymography of T98G NC and T98G-*ARHGAP21*-knockdown cell supernatants, collected after 48 h of growth in serum-free medium. (B) Graphic showing the quantitation of MMP-2 pro and active isoforms. (C) Gelatin zymography of T98G NC and T98G-*ARHGAP21*-knockdown cells cultivated on poly-lysine or Matrigel-coated plates for 48 h, showing the increased MMP-2 secretion, due to ARHGAP21 depletion. (D) T98G NC and T98G-*ARHGAP21* knockdown cells were submitted to migration experiments on transwells (8 μm pore) for 48 h, and presented increased migration properties. Increased migration rates from all clones were statistically significant (Wilcoxon Rank Sum Test; $*p<0.05$).

inhibited clones (data not shown). Nevertheless, Cdc42 activity was found mainly in ARHGAP21-depleted cells (Fig. 5A).

Moreover, Cdc42 translocates to membrane protrusion regions and to perinuclear area, colocalizing with actin dots in *ARHGAP21*-knockdown cells, following F-actin changes (Fig. 5C, yellow arrow heads and yellow regions in merge frames). The quantification of Cdc42 displacement evidenced that this feature is raised due to ARHGAP21 depletion (Fig. 5B). Results shown are representative of all ARHGAP21-depleted clones analyzed.

### 3.6. ARHGAP21 depletion increases MMP-2 secretion and migration rates

As FAK is known to promote MMP-2 and MMP-9 production when it's phosphorylated in tyrosines 397 and 925 [21,22], which are hyper-phosphorylated when ARHGAP21 is depleted, and since Cdc42 activity has recently been linked to MMP-2 activation [23], we checked the secretion of gelatinolityc MMPs from *ARHGAP21*-knockdown cells. Gelatin zymography experiments [24], using supernatants of T98G NC and *ARHGAP21*-knockdown cells cultivated in serum-free medium for 48 h, displayed increased MMP-2 secretion and its slightly activation when ARHGAP21 was depleted (Fig. 6A). Pro-MMP-2 (72KDa form) and active MMP-2 (64KDa) secretion was increased in all inhibited clones (Fig. 6A and B, graph). The cultivation of these cell lines in basement membrane matrix (Matrigel™ BD Bioscience) for 48 h induces increased MMP-2 secretion in *ARHGAP21*-knockdown cells in comparison to the parental T98G-NC cells (Fig. 6B). Since this condition mimics an activation of ECM-cell signaling, these results evidenced that ARHGAP21 mediates ECM-cell communication.

As cell movement through tissues has been observed to play a primary role in cancer progression, we evaluated the migration capacity of ARHGAP21-depleted cells. Migration assays were carried out in Costar Transwells, whose membranes were coated with poly-L-lysine, in triplicate. Cells have been serum starved before the 48 h migration assays and differential proliferative rates between clones have been diminished through measuring the absorbance of filters with the total content of cells (upper and bottom membrane cells) and using this to calculate the percentage of migrated cells. Results shown are means of at least 2 independent experiments. T98G NC cells

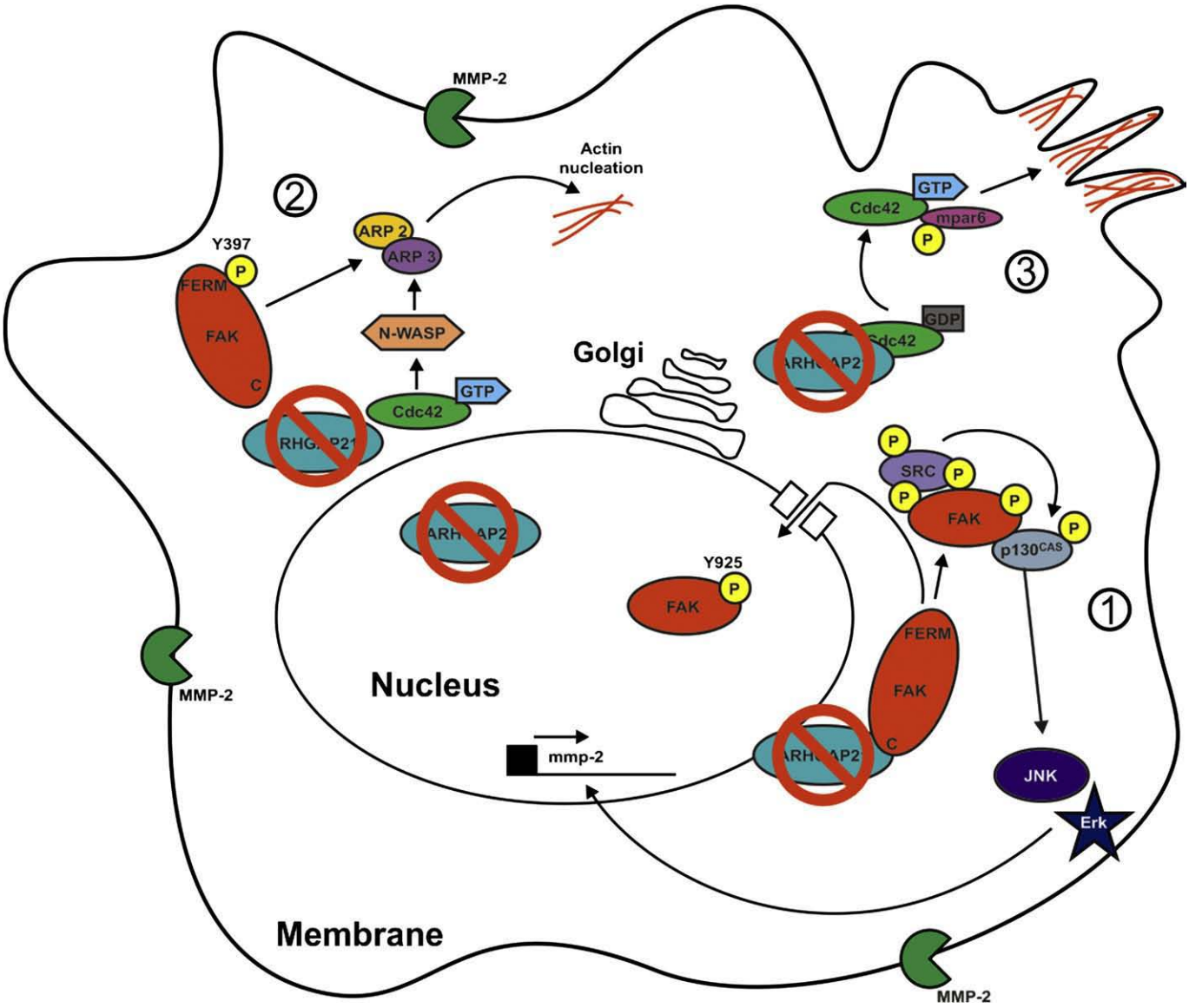


**Fig. 7.** Schematic ARHGAP21 action mechanism. ARHGAP21 is a nuclear and perinuclear protein that interacts with FAK in the perinuclear region of glioblastoma cells. ARHGAP21 depletion by shRNAi causes: (1) FAK phosphorylation on Y397 and Y925 that leads to $p130^{CAS}$ binding and its activation by Src, which, consequently, results in the activation of JNK and ERK as transcription factors that induce mmp-2 gene transcription, and, ultimately, MMP-2 secretion increases; (2) FAK phosphorylation on Y397 liberates Arp2/3 and allows them to be activated by Cdc42-GTP, resulting in increased actin nucleation; (3) Cdc42-GTP interacts with mPar6 and atypical PKCs at the leading edge to develop membrane protrusions using nascent actin filaments.

displayed a mean migration rate (mr) of 30.67% ± 11.22 while sh1 inhibited clones #3 and #15 displayed mr of 62.78 ± 26.09% and mr of 46.4 ± 6.78%, respectively, and sh2 inhibited ones, #2 and #16, displayed mr of 51.83 ± 7.52% and mr of 77.83 ± 4.07%, respectively (Fig. 6D). Pictures displayed are examples of stained-filters of each clone after the period of migration.

Our results show significant differences ($p<0.05$) between T98G NC and *ARHGAP21*-knockdown cells, suggesting that ARHGAP21 might play an important role controlling glioblastoma cell migration.

## 4. Discussion

In this report we showed that ARHGAP21 is localized to the nucleus and perinuclear region of several cell lines. Recently, our group characterized ARHGAP21 translocation from the nucleus to the membrane due to cardiac pressure overload [19]. In contrast to our data on cardiomyocytes, we found no stimuli leading to ARHGAP21 translocation from the nuclei in glioblastoma cell lines, which we hypothesize to be due to the malignant character of those cells. Our results also contrast to data described by Dubois and Chavrier [8] in which the authors described only Golgi-localized ARHGAP21. We concluded that the different results obtained by the two research groups were due to the permeabilization protocol used: their saponin permeabilization *versus* our Triton-X-100 protocol (Supplementary material, Sup.Fig.2A). Indeed in support of our data, Sousa et al. [20] showed ARHGAP21 nuclear staining in Caco-2 and JEG-3 epithelial cell lines. ARHGAP21 nuclear function remains unclear however should be clarified soon.

We also demonstrated, herein, an interaction between ARHGAP21 and the Focal adhesion kinase (FAK) in glioblastoma cell lines (T98G and U138MG) that occurs in the perinuclear region. FAK is known to promote cell migration through several signaling pathways. One of these pathways uses the "CAS" (Crk-associated substrate) family of proteins that include $p130^{CAS}$. The $p130^{CAS}$-SH3 domain mediates its association with the FAK PR2 and PR3 region (proline-rich regions 2 and 3), and this association promotes its phosphorylation by Src. Phosphorylated $p130^{CAS}$ recruits Crk adaptor proteins, which results in Rac1, Cdc42 or JNK activation and ultimately promotes membrane protrusions and cell migration [25,26]. Therefore, the interaction between ARHGAP21 and the C-terminal region of FAK might inhibit $p130^{CAS}$ association to the PR3 region, consequently blocking FAK phosphorylation by Src and the activation of downstream signaling (Fig. 7, item 1).

Depletion of ARHGAP21 drastically changes T98G cellular morphology and results in cytoskeleton rearrangement. This was characterized by loss of cortical actin, accumulation of perinuclear actin dots, formation of membrane protrusions and by the activation of Cdc42, in parallel with FAK (Fig. 7, item 3). The perinuclear accumulation of both actin and Cdc42 probably results from increased actin nucleation on Golgi membranes, as described by Dubois et al. [8]. Since Cdc42 activity has been reported to be also dependent on FAK, as FAK-knockdown reduces its activation and, activation of $p130^{CAS}$ results in Cdc42 activation [25,26], ARHGAP21 may exert a dual control over Cdc42: through its GAP activity and by blocking $p130^{CAS}$ activation, downstream of FAK.

In addition, the action of ARHGAP21 on Cdc42 has previously been reported to be important in the control of the Arp2/3 complex and the F-actin dynamics on Golgi membranes [8]. Interestingly, the FAK-FERM domain binds to the Arp2/3 complex, however FAK Tyr397 phosphorylation triggers dissociation of the dynamic FAK–Arp3 complex and results in activation of Arp3, necessary for developing cell protrusions [27]. It has been suggested that the Arp2/3-FAK complex is released when Arp3 is activated by active Cdc42, thus enabling FAK phosphorylation. Surprisingly, our results corroborate this hypothesis, as loss of ARHGAP21 increases Cdc42 activity, which is then able to increase Arp3 activity and, consequently, release it from FAK leading, ultimately, to the FAK Tyr397 phosphorylation that we observed (Fig. 7, item 2). Moreover, since the interaction between ARHGAP21 and FAK occurs in the perinuclear region, we hypothesize that ARHGAP21 sequesters FAK in this inactive state, as ARHGAP21 depletion increases FAK Y925 phosphorylation and results in its translocation to the nuclear compartment. Although this translocation was not expected since FAK nuclear accumulation is not linked to its kinase activity [28], GFP-FAT construct, in which the Tyr 925 resides, was shown to accumulate in the nucleus [29] and stress stimuli or disruption of cell adhesion trigger FAK nuclear accumulation [30]. Thus, as ARHGAP21 depletion changes adherens junctions composition [20] there is a possibility that, FAK behaves differently in tumor cells.

Astrocytic brain tumors, of which glioblastoma multiforme is the most malignant, express high levels of FAK [31]. The invasion of adjacent brain sites is mediated mainly through the secretion of matrix metalloproteases (MMPs), a family of enzymes capable of degrading many components of the extracellular matrix, such as collagen, fibronectin and proteoglycans [32]. It has been reported that, in glioblastoma cell lines, angiopoetin-2 induces increased production of MMP-2 through activation of FAK→$p130^{CAS}$ [33]. Furthermore, FAK depletion in head and neck squamous carcinoma cells reduces invasion via downregulation of MMP-2 expression [34]. Given that depletion of ARHGAP21 induces higher MMP-2 secretion, as seen in epithelial to mesenchymal transition (EMT), ARHGAP21 might be an essential modulator of glioblastoma multiforme progression through action upon Cdc42 and FAK.

Taken together the above results suggest that ARHGAP21 inhibits glioblastoma cell migration. This inhibition is mediated by (1) ARHGAP21 negative regulation of Cdc42, (2) of FAK→$p130^{CAS}$ signaling inactivation, and (3) a decreased secretion of metalloprotease-2. Those results not only suggest that ARHGAP21 might control glioblastoma aggressiveness, but also indicate that ARHGAP21 might be a master regulator of migration in different tissues and, as such, have a crucial role in the control of the progression of different tumor types.

## Acknowledgements

This work was supported by Fundação de Amparo à Pesquisa do Estado de São Paulo (FAPESP) and the Conselho Nacional de Desenvolvimento Científico e Tecnológico (CNPq). We thank Dr. David Sacks from Brigham and Women's Hospital for the donation of the plasmid encoding WBD-GST protein, Dr. Pascale Cossart for the N- and C-terminus ARHGAP21 constructs and Dr. Carla Franco-Penteado for the help with zymography experiments. We are also thankful to Dr. Nicola Conran, Dr. Letícia Froelich-Archangelo and Rachel Foglio for English revision of the manuscript.

## Appendix A. Supplementary data

Supplementary data associated with this article can be found, in the online version, at doi:10.1016/j.bbamcr.2009.02.010.

## References

[1] S.K. Mitra, D.A. Hanson, D.D. Schlaepfer, Focal adhesion kinase: in command and control of cell motility, Nat. Rev. Mol. Cell Biol. 6 (2005) 56–68.
[2] Y. Zheng, Dbl family guanine nucleotide exchange factors, Trends Biochem. Sci. 26 (2001) 724–732.
[3] B. Olofsson, Rho guanine dissociation inhibitors: pivotal molecules in cellular signalling, Cell. Signal. 11 (1999) 545–554.
[4] N. Lamarche, A. Hall, GAPs for rho-related GTPases, Trends Genet. 10 (1994) 436–440.
[5] R.P. Kandpal, Rho GTPase activating proteins in cancer phenotypes, Curr. Protein Pept. Sci. 7 (2006) 355–365.
[6] D.S. Basseres, E.V. Tizzei, A.A. Duarte, F.F. Costa, S.T. Saad, ARHGAP10, a novel human gene coding for a potentially cytoskeletal Rho-GTPase activating protein, Biochem. Biophys. Res. Commun. 294 (2002) 579–585.
[7] C. Nourry, S.G. Grant, J.P. Borg, PDZ domain proteins: plug and play! Sci. STKE 2003 (2003) RE7.

[8] T. Dubois, P. Chavrier, ARHGAP10, a novel RhoGAP at the cross-road between ARF1 and Cdc42 pathways, regulates Arp2/3 complex and actin dynamics on Golgi membranes, Med. Sci. (Paris) 21 (2005) 692–694.
[9] P. Kleihues, D.N. Louis, B.W. Scheithauer, L.B. Rorke, G. Reifenberger, P.C. Burger, W.K. Cavenee, The WHO classification of tumors of the nervous system, J. Neuropathol. Exp. Neurol. 61 (2002) 215–225 discussion 226–219.
[10] R. Stupp, M.E. Hegi, M.J. van den Bent, W.P. Mason, M. Weller, R.O. Mirimanoff, J.G. Cairncross, Changing paradigms—an update on the multidisciplinary management of malignant glioma, Oncologist 11 (2006) 165–180.
[11] L.A. Stewart, Chemotherapy in adult high-grade glioma: a systematic review and meta-analysis of individual patient data from 12 randomised trials, Lancet 359 (2002) 1011–1018.
[12] S. Povey, R. Lovering, E. Bruford, M. Wright, M. Lush, H. Wain, The HUGO Gene Nomenclature Committee (HGNC), Hum. Genet. 109 (2001) 678–680.
[13] X.D. Ren, W.B. Kiosses, M.A. Schwartz, Regulation of the small GTP-binding protein Rho by cell adhesion and the cytoskeleton, EMBO J. 18 (1999) 578–585.
[14] L.A. Cooper, T.L. Shen, J.L. Guan, Regulation of focal adhesion kinase by its amino-terminal domain through an autoinhibitory interaction, Mol. Cell. Biol. 23 (2003) 8030–8041.
[15] M.D. Schaller, C.A. Otey, J.D. Hildebrand, J.T. Parsons, Focal adhesion kinase and paxillin bind to peptides mimicking beta integrin cytoplasmic domains, J. Cell Biol. 130 (1995) 1181–1187.
[16] E.E. Sander, S. van Delft, J.P. ten Klooster, T. Reid, R.A. van der Kammen, F. Michiels, J.G. Collard, Matrix-dependent Tiam1/Rac signaling in epithelial cells promotes either cell–cell adhesion or cell migration and is regulated by phosphatidylinositol 3-kinase, J. Cell Biol. 143 (1998) 1385–1398.
[17] S.H. Kim, Z. Li, D.B. Sacks, E-cadherin-mediated cell–cell attachment activates Cdc42, J. Biol. Chem. 275 (2000) 36999–37005.
[18] D. Muir, L. Sukhu, J. Johnson, M.A. Lahorra, B.L. Maria, Quantitative methods for scoring cell migration and invasion in filter-based assays, Anal. Biochem. 215 (1993) 104–109.
[19] L. Borges, C.L. Bigarella, M.O. Baratti, D.P. Crosara-Alberto, P.P. Joazeiro, K.G. Franchini, F.F. Costa, S.T. Saad, ARHGAP21 associates with FAK and PKCzeta and is redistributed after cardiac pressure overload, Biochem. Biophys. Res. Commun. 374 (2008) 641–646.
[20] S. Sousa, D. Cabanes, C. Archambaud, F. Colland, E. Lemichez, M. Popoff, S. Boisson-Dupuis, E. Gouin, M. Lecuit, P. Legrain, P. Cossart, ARHGAP10 is necessary for alpha-catenin recruitment at adherens junctions and for *Listeria* invasion, Nat. Cell Biol. 7 (2005) 954–960.
[21] D. Dang, J.R. Bamburg, D.M. Ramos, Alphavbeta3 integrin and cofilin modulate K1735 melanoma cell invasion, Exp. Cell Res. 312 (2006) 468–477.
[22] N.N. Mon, H. Hasegawa, A.A. Thant, P. Huang, Y. Tanimura, T. Senga, M. Hamaguchi, A role for focal adhesion kinase signaling in tumor necrosis factor-alpha-dependent matrix metalloproteinase-9 production in a cholangiocarcinoma cell line, CCKS1, Cancer Res. 66 (2006) 6778–6784.
[23] E. Ispanovic, D. Serio, T.L. Haas, Cdc42 and RhoA have opposing roles in regulating Membrane Type 1-Matrix Metalloproteinase localization and Matrix Metalloproteinase-2 activation, Am. J. Physiol. Cell Physiol. 295 (3) (2008) C600–C610.
[24] F. Capon, H. Emonard, W. Hornebeck, F.X. Maquart, P. Bernard, Expression and activation of pro-gelatinase A by human melanoma cell lines with different tumorigenic potential, Clin. Exp. Metastasis 17 (1999) 463–469.
[25] B.D. Cox, M. Natarajan, M.R. Stettner, C.L. Gladson, New concepts regarding focal adhesion kinase promotion of cell migration and proliferation, J. Cell. Biochem. 99 (2006) 35–52.
[26] D.A. Hsia, S.K. Mitra, C.R. Hauck, D.N. Streblow, J.A. Nelson, D. Ilic, S. Huang, E. Li, G.R. Nemerow, J. Leng, K.S. Spencer, D.A. Cheresh, D.D. Schlaepfer, Differential regulation of cell motility and invasion by FAK, J. Cell Biol. 160 (2003) 753–767.
[27] B. Serrels, A. Serrels, V.G. Brunton, M. Holt, G.W. McLean, C.H. Gray, G.E. Jones, M.C. Frame, Focal adhesion kinase controls actin assembly via a FERM-mediated interaction with the Arp2/3 complex, Nat. Cell Biol. 9 (2007) 1046–1056.
[28] S.T. Lim, X.L. Chen, Y. Lim, D.A. Hanson, T.T. Vo, K. Howerton, N. Larocque, S.J. Fisher, D.D. Schlaepfer, D. Ilic, Nuclear FAK promotes cell proliferation and survival through FERM-enhanced p53 degradation, Mol. Cell 29 (2008) 9–22.
[29] B. Kovacic-Milivojevic, F. Roediger, E.A. Almeida, C.H. Damsky, D.G. Gardner, D. Ilic, Focal adhesion kinase and p130Cas mediate both sarcomeric organization and activation of genes associated with cardiac myocyte hypertrophy, Mol. Biol. Cell. 12 (2001) 2290–2307.
[30] S.T. Lim, D. Mikolon, D.G. Stupack, D.D. Schlaepfer, FERM control of FAK function: implications for cancer therapy, Cell Cycle 7 (2008) 2306–2314.
[31] J.A. Girault, A. Costa, P. Derkinderen, J.M. Studler, M. Toutant, FAK and PYK2/CAKbeta in the nervous system: a link between neuronal activity, plasticity and survival? Trends Neurosci. 22 (1999) 257–263.
[32] J.S. Rao, P.A. Steck, S. Mohanam, W.G. Stetler-Stevenson, L.A. Liotta, R. Sawaya, Elevated levels of M(r) 92,000 type IV collagenase in human brain tumors, Cancer Res. 53 (1993) 2208–2211.
[33] B. Hu, M.J. Jarzynka, P. Guo, Y. Imanishi, D.D. Schlaepfer, S.Y. Cheng, Angiopoietin 2 induces glioma cell invasion by stimulating matrix metalloprotease 2 expression through the alphavbeta1 integrin and focal adhesion kinase signaling pathway, Cancer Res. 66 (2006) 775–783.
[34] M. Canel, P. Secades, M. Garzon-Arango, E. Allonca, C. Suarez, A. Serrels, M. Frame, V. Brunton, M.D. Chiara, Involvement of focal adhesion kinase in cellular invasion of head and neck squamous cell carcinomas via regulation of MMP-2 expression, Br. J. Cancer 98 (2008) 1274–1284.